DALTON

Density-functional study of the ground- and excited-spin states of $[M_2Cl_9]^{3-}$ (M = Mo or W) face-shared dimers: consequences for structural variation in $A_3M_2Cl_9$ complexes†

Robert Stranger,*[a] Stuart A. Macgregor,[b] Timothy Lovell,[a] John E. McGrady[a] and Graham A. Heath[b]

[a] *The Department of Chemistry, Faculties, The Australian National University, Canberra, ACT 0200, Australia*

[b] *The Research School of Chemistry, The Australian National University, Canberra, ACT 0200, Australia*

The optimized geometries and relative energies for the ground- and excited-spin states (S_{max} = 0–3) of $[M_2Cl_9]^{3-}$ (M = Mo or W) have been determined from density-functional calculations. For both systems the calculations predict a dramatic increase in metal–metal distance, with a corresponding increase in M–Cl_b–M bridge angle, as the dimer spin state (S_{max}) increases. The terminal MCl_3 groups on the other hand are relatively insensitive to changes in the M–M separation. For both $[Mo_2Cl_9]^{3-}$ and $[W_2Cl_9]^{3-}$ the spin-singlet structure (S_{max} = 0) is predicted to be the most stable species when using the local-density approximation (LDA), in agreement with experiment. In contrast, when non-local gradient corrections to the total energy are incorporated, both the spin-quintet (S_{max} = 2) and -septet (S_{max} = 3) species are predicted to be more stable than the spin singlet for $[Mo_2Cl_9]^{3-}$. The calculated (LDA) singlet geometry for $[W_2Cl_9]^{3-}$ is in very good agreement with the observed structure whereas for $[Mo_2Cl_9]^{3-}$ the geometry of the spin-triplet species is closer to experiment. Incorporation of relativistic effects is more significant for $[W_2Cl_9]^{3-}$ resulting in a further destabilization of the higher-spin states, particularly the spin-quintet and -septet species, relative to the singlet configuration. Fragment analysis showed that the metal–metal and metal–bridge contributions to the total bonding in the higher-spin species counteract each other. The destabilization due to loss of metal–metal bonding in the higher-spin states is greater than the stabilization gained from the enhanced metal–bridge interaction. However, the reduction in the M–M interaction is more pronounced for $[W_2Cl_9]^{3-}$ and thus its higher-spin states are less accessible than for $[Mo_2Cl_9]^{3-}$, accounting for the more dramatic variation in M–M distances observed in $A_3Mo_2Cl_9$ complexes.

Bioctahedral face-shared M_2L_9 dimers are known for most of the transition metals and exhibit a wide variety of structural and electronic behaviour.[1] Of particular interest to theoreticians has been the description of the metal–metal interactions in these species which are fundamental to their structural, magnetic and spectroscopic properties. Cotton and Ucko[2] have provided a classification of face-shared systems based on the geometry of the ideal confacial bioctahedron **1**, which features an M–L_b–M angle, β, of 70.5° with each metal equidistant between the planes defined by the three terminal ligands and the three bridging ligands. In general, M_2L_9 species may either be compressed (β < 70.5°) or elongated (β > 70.5°) relative to this ideal case.

The extremes of geometry and metal–metal interaction are exemplified by the nonahalogenodimetalates of the chromium triad. The Cr–Cr distance in $Cs_3Cr_2Cl_9$ is 3.12 Å, the elongated structure suggesting a very weak metal–metal interaction.[3] This is confirmed by magnetic measurements which indicate the presence of three unpaired electrons per Cr atom. In contrast, the $[W_2Cl_9]^{3-}$ anion is compressed with a W–W distance of 2.41 Å for the potassium salt,[4] indicative of strong metal–metal bonding. The molybdenum analogue, $[Mo_2Cl_9]^{3-}$, exhibits intermediate behaviour between that of the chromium and tungsten species and, because of this, has been the subject of a number of detailed studies into its spectroscopic, magnetic and structural properties.[5] The intermediate nature of the metal–metal interaction is particularly apparent in the structural data for $A_3Mo_2Cl_9$ complexes (A = K, Cs, Rb, NH_4 or NMe_4) in

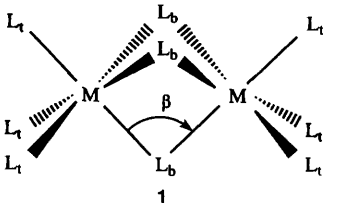

1

which the geometry of the $[Mo_2Cl_9]^{3-}$ anion is strongly dependent on the size of the univalent cation, A, with the Mo–Mo distances ranging from 2.52 (A = K^+) to 2.78 Å (A = NMe_4^+).[5b] These data indicate that changes in the close-packing arrangement are sufficient to cause significant variation of the Mo–Mo distance, thus influencing the extent of Mo–Mo interaction. This latter point is reflected in the measured ground-state exchange coupling constant, $-J_{ab}$, for these species which reduces with increased Mo–Mo separation.[5g] The detailed spectroscopic investigation[5c-f] of $Cs_3Mo_2X_9$ (X = Cl or Br), coupled with broken-symmetry Xα-SW density-functional calculations,[6] have indicated that the Mo–Mo σ bond is not fully optimized and undoubtedly this facilitates the structural variation observed in the $[Mo_2X_9]^{3-}$ series. Comparison of the potassium and caesium salts of $[Mo_2Cl_9]^{3-}$ and $[W_2Cl_9]^{3-}$ shows the cation dependency to be smaller for the tungsten system,[5b] implying that the metal–metal bonding in $[W_2X_9]^{3-}$ is stronger.

A number of theoretical studies on $[M_2X_9]^{3-}$ species have

† *Non-SI units employed:* cal = 4.184 J, eV ≈ 1.60 × 10^{-19} J.

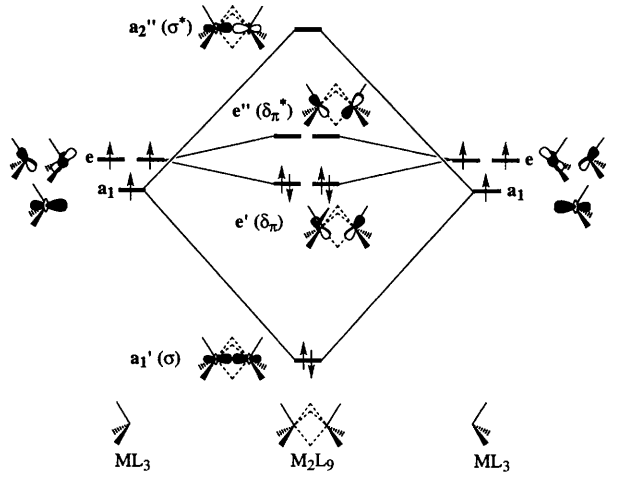

Fig. 1 Schematic representation of the metal–metal manifold in M_2L_9 species derived from two conical ML_3 fragments. Contributions from bridging ligands are omitted for clarity. The occupation indicated is equivalent to that of spin-singlet $[M_2L_9]^{3-}$ (M = Mo or W)

been published.[6–12] Summerville and Hoffmann[7] have discussed the structures of M_2L_9 face-shared dimers in general using the extended-Hückel methodology. In their study the analysis of direct metal–metal interactions was based on the interaction of two conical ML_3 units. For such a fragment, the metal-based t_{2g} orbitals of an ideal octahedron are split into a single orbital of σ symmetry with respect to the metal–metal axis and a doubly degenerate pair with $\frac{2}{3}\delta$ and $\frac{1}{3}\pi$ character.[8] In the bioctahedron, combinations of these ML_3 fragment orbitals result in a manifold of bonding (σ, δ_π) and antibonding (δ_π* and σ*) metal-based orbitals (see Fig. 1). In the case of a weak M–M interaction the splitting of the δ_π and δ_π* orbitals is small and a high-spin configuration may become favoured. Summerville and Hoffmann also emphasized the importance of distortions intrinsic to the monomer units and the role of the metal–bridge interaction in determining the geometry of M_2L_9 species. Very recently, Cotton and Feng[11] have undertaken *ab initio* configuration interaction (CI) calculations on $[Mo_2Cl_9]^{3-}$ in order to study the effects of metal–metal bonding on the low-lying excited states.

Density-functional methods[13] have also been used to study the magnetic exchange interaction in $[Mo_2X_9]^{3-}$ species. Ginsberg[9] applied the Xα-SW approach to study the effect of the Mo–Mo separation in $[Mo_2Cl_9]^{3-}$ and this work was more recently extended by Medley and Stranger[6] who employed the Xα-VB broken-symmetry formalism in the study of $[Mo_2X_9]^{3-}$ (X = Cl, Br or I). Ziegler and co-workers[10] have studied the effects of chloride substitution by thioethers in both the bridging and terminal positions of $[Mo_2Cl_9]^{3-}$. We have also recently published a communication indicating the importance of broken-symmetry in describing weakly and intermediately coupled bimetallic systems.[12] The energy of the broken-symmetry state, however, is a weighted average of the energies of the pure spin states corresponding to S_{max} = 0–3 in the present case. In this contribution we intend to analyse the factors which determine the stabilities of these pure spin states. Since such an analysis necessitates a fragment-based approach we are restricted to using full-symmetry methods.

In this study, density-functional theory is used to calculate the optimum geometries and relative energies for the ground and excited spin states (S_{max} = 0–3) resulting from the coupling of the two single-ion ($S = \frac{3}{2}$) spins in $[M_2Cl_9]^{3-}$ (M = Mo or W). The S_{max} = 0, 1, 2 and 3 spin levels arise from the orbital configurations $\sigma^2\delta_\pi^4$, $\sigma^2\delta_\pi^3\delta_\pi^{*1}$, $\sigma^2\delta_\pi^2\delta_\pi^{*2}$ and $\sigma^1\delta_\pi^2\delta_\pi^{*2}\sigma^{*1}$, respectively. It should be noted, however, that the $\sigma^2\delta_\pi^3\delta_\pi^{*1}$ configuration gives rise to several spin-triplet states and, consequently, the optimized geometry for this orbital configuration will necessarily be an average of these states. The geometries of both $[Mo_2Cl_9]^{3-}$ and $[W_2Cl_9]^{3-}$ show a marked dependence on the univalent cation, A, in $A_3M_2Cl_9$ complexes, although this effect is significantly larger in the molybdenum system. By computing the relative energies and geometries for the excited spin states it should be possible to assess the relative contributions of these levels to the overall electronic structure of these systems. A fragment approach will also be adopted to rationalize the trends in relative energies of the excited spin levels of $[Mo_2Cl_9]^{3-}$ and $[W_2Cl_9]^{3-}$.

Computational Details

Calculations employed the Amsterdam density functional (ADF) package (version 2.0.1) developed by Baerends *et al.*[14] and utilizing the numerical integration scheme of te Velde and co-workers.[15] Triple-ζ STO (slater orbital) basis sets were employed for Mo and W and a double-ζ STO basis set extended with a polarization function was chosen for Cl.[16] An auxiliary set of s, p, d, f and g STO basis functions centred on all nuclei was used in order to fit the molecular density and describe accurately the coulomb and exchange potentials in each SCF (self-consistent field) cycle.[17] Core electrons (up to and including 4p for Mo, 5p for W and 2p for Cl) were treated using the frozen-core approximation.[18] The local-density approximation[19] (LDA) was employed using the parameterization of Vosko *et al.*[20] Geometry optimizations were undertaken on the basis of D_{3h} molecular symmetry using the method developed by Versluis and Ziegler.[21] Those incorporating the quasi-relativistic correction of Ziegler *et al.*[22] were also undertaken. The energies of all LDA-optimized species were recalculated to include the non-local (NL) gradient corrections of Perdew *et al.*[23] as well as the quasi-relativistic correction of Ziegler *et al.* All fragment calculations included NL gradient and quasi-relativistic corrections. Spin-unrestricted calculations were performed on all open-shell $[M_2Cl_9]^{3-}$ species. All calculations were made on either an IBM 3AT or SUN UltraSparc 170 computer.

Results and Discussion

Optimized geometries

The geometries of $[Mo_2Cl_9]^{3-}$ and $[W_2Cl_9]^{3-}$, optimized using the local-density approximation for different electron occupations of the metal–metal manifold, are given in Table 1. For both systems the geometries were optimized both with and without the quasi-relativistic correction. It is clear that for both metals unpairing the electron spin density and occupation of the higher-lying, formally M–M antibonding orbitals, results in significant changes in the molecular geometry. The trends in geometry variation are, however, similar for both metals. For $[Mo_2Cl_9]^{3-}$ a steady increase in the Mo–Mo separation is calculated as the total spin increases from 2.288 (S_{max} = 0) to 2.612 (1) and 2.868 Å (2). These Mo–Mo distances are quite similar to those reported by Ziegler and co-workers[10] for the thioether-substituted face-shared dimer $[(SH_2)Cl_2Mo(\mu\text{-}Cl_3)MoCl_2(SH_2)]^-$. Unpairing the a_1' electron pair (S_{max} = 3) results in a significant further lengthening of the Mo–Mo distance to 3.454 Å. Overall the calculations predict an increase of nearly 1.2 Å in the Mo–Mo distance in going from the spin-singlet to the spin-septet species. The large changes in the Mo–Mo distance are reflected in the Mo–Cl_b–Mo bridge angle which also increases with the total spin. Similar trends are seen in the geometries calculated for $[W_2Cl_9]^{3-}$, with the W–W distance increasing from 2.404 Å for the spin-singlet species to 3.534 Å for the spin septet. Other calculated parameters exhibit only minor changes. In particular, the terminal $\{MCl_3\}$ unit seems insensitive to changes in the M–M separation, as is observed from the experimental data given in Table 2. For both

Table 1 Optimized geometries and total energies for the ground- and excited-state spin species of $[M_2Cl_9]^{3-}$ (M = Mo or W)

Spin state	M	Structural parameters (Å, °)[a] M–M	M–Cl_t	M–Cl_b	M–Cl_b–M	M–M–Cl_t	Total energy[a,b]/eV LDA	LDA + NL
Singlet	Mo	2.288 (2.288)	2.467 (2.460)	2.529 (2.523)	53.78 (53.92)	123.9 (123.7)	−49.995 (−50.528)	−43.780 (−44.285)
	W	2.404 (2.354)	2.501 (2.482)	2.591 (2.575)	55.28 (54.38)	123.4 (122.1)	−51.355 (−48.932)	−45.349 (−42.763)
Triplet	Mo	2.612 (2.592)	2.458 (2.452)	2.509 (2.504)	62.73 (62.33)	125.2 (125.1)	−49.166 (−49.640)	−43.224 (−43.658)
	W	2.696 (2.616)	2.495 (2.474)	2.564 (2.553)	63.43 (61.63)	125.4 (124.9)	−50.458 (−47.779)	−44.686 (−41.844)
Quintet	Mo	2.868 (2.850)	2.462 (2.456)	2.495 (2.486)	70.16 (69.95)	125.1 (125.1)	−49.573 (−49.990)	−44.043 (−44.421)
	W	2.930 (2.874)	2.502 (2.478)	2.542 (2.524)	70.38 (69.40)	125.3 (125.0)	−50.734 (−47.852)	−45.338 (−42.303)
Septet	Mo	3.454 (3.446)	2.444 (2.438)	2.557 (2.549)	84.97 (85.05)	123.1 (123.1)	−49.312 (−49.591)	−44.293 (−44.591)
	W	3.534 (3.508)	2.486 (2.463)	2.597 (2.569)	85.75 (86.11)	123.4 (123.6)	−50.251 (−47.130)	−45.343 (−42.067)

[a] Structural parameters and total energies calculated using the quasi-relativistic correction of Ziegler *et al.*[22] are given in parentheses. [b] Calculated using the local-density approximation with or without the non-local gradient corrections of Perdew *et al.*[23]

Table 2 Experimental data for $A_3M_2Cl_9$ (M = Mo or W) complexes[5b]

A	Structural parameters (Å, °) M–M	M–Cl_t	M–Cl_b	M–Cl_b–M
$A_3Mo_2Cl_9$				
K	2.524	2.400	2.50	60.6
Rb	2.590	2.411	2.480	63.0
NH_4	2.600	2.398	2.471	63.5
Cs	2.67	2.41	2.49	64.8
NMe_4	2.778	2.363	2.480	68.1
$A_3W_2Cl_9$				
K	2.409	2.40	2.48	58.1
Cs	2.50	2.407	2.448	61.4

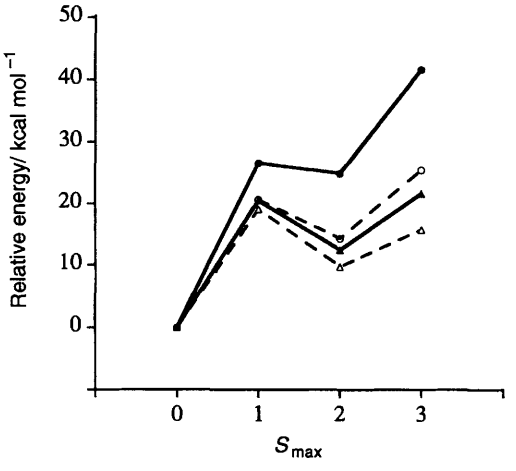

Fig. 2 Relative energy (LDA) *vs.* total spin for $[M_2Cl_9]^{3-}$ [M = Mo (▲) or W (●)] systems calculated with and without (△, ○) the quasi-relativistic correction

metals, and particularly for M = W, the M–Cl_t and M–Cl_b bonds are calculated to be somewhat longer than those found experimentally. This overestimation of metal–ligand bonds is contrary to experience using the LDA at this level,[13b,24] but has been noted before in other systems featuring several anionic π-donor ligands.[25] Inclusion of relativistic effects has only a small effect on the calculated geometries of $[Mo_2Cl_9]^{3-}$, with the Mo–Mo separation being at most only 0.02 Å shorter. However, for $[W_2Cl_9]^{3-}$ the effect is more significant with the W–W separation being up to 0.08 Å shorter. The shorter M–M distances obtained from the relativistic calculations result from the greater contribution of the metal 5s (Mo) and 6s (W) orbitals to the M–M σ bonding.

Relative energies of spin states

Fig. 2 plots the relative energies (LDA), calculated both with and without the relativistic correction, against total spin for $[Mo_2Cl_9]^{3-}$ and $[W_2Cl_9]^{3-}$. In each of the four plots in Fig. 2 the energy of the spin-singlet geometry is placed at an arbitrary zero. Neglecting relativistic effects, the relative changes in energy with spin state are very similar for both metals. The relative energies for the S_{max} = 0–2 states are also similar to those calculated by Ziegler and co-workers[10] for the thioether-substituted face-shared molybdenum dimer. As expected, incorporation of relativistic effects is more significant for $[W_2Cl_9]^{3-}$, although the shifts in relative energy are not negligible for the molybdenum system, particularly for the higher spin states. The largest correction occurs in both metals for S_{max} = 3 and is due to the contribution of the metal s-electron density in the $a_1'(\sigma)$ and $a_2''(\sigma^*)$ orbitals which are both singly occupied for this electron configuration. For both metals the spin-singlet species is calculated to be the most stable. For $[W_2Cl_9]^{3-}$ the calculated geometry of the spin-singlet species agrees well with that found experimentally (see Table 2).[4,5b] The shortest Mo–Mo distance of 2.524 Å for $[Mo_2Cl_9]^{3-}$ occurs for the potassium salt, therefore the calculated Mo–Mo distance of 2.288 Å for the spin-singlet species is about 0.2 Å too short. However, magnetic and spectroscopic studies[5] indicate that only the $a_1'(\sigma)$ orbital is involved in strong metal–metal bonding, thus the experimental geometry should be better reflected in the calculated geometries for the spin-triplet and, possibly, -quintet species. Given the experimental range of Mo–Mo distances between 2.52 and 2.78 Å, the calculated spin-triplet value of 2.61 Å is quite acceptable whereas the spin-quintet value of 2.87 Å is too long.

From Table 1 and Fig. 3 it is clear that the inclusion of non-local gradient corrections to the total energy results in a stabilization of the higher-spin species relative to the spin singlet for both Mo and W. In fact, for $[Mo_2Cl_9]^{3-}$, both the S_{max} = 2 and 3 species are predicted to be more stable than the spin singlet. In the absence of relativistic corrections, even the S_{max} = 3 species of $[W_2Cl_9]^{3-}$ is predicted to be almost comparable in energy to the spin singlet. These results are contrary to the experimental data which clearly establish a spin-singlet ground state for both Mo and W.[5] Thus, it would appear that the LDA calculated energies better reflect the experimental data, at least in terms of the relative energies of the ground and excited spin species, whereas the non-local gradient corrections overestimate the stability of the higher-spin states, in particular for the S_{max} = 2 and 3 species.

While the absolute energies of the different spin states may be incorrect, on the basis of Fig. 3 it is reasonable to compare the calculated trends in relative energy for the molybdenum and tungsten systems since the non-local gradient corrections effectively stabilize the excited spin states in both systems to the same extent. Unpairing one of the e′ (δ_π) electron pairs to give

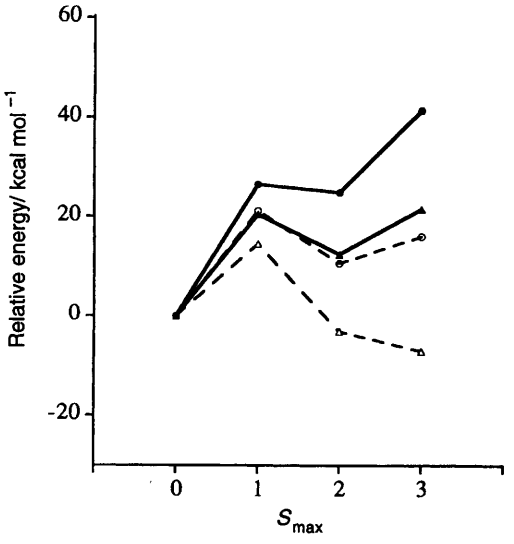

Fig. 3 Relative energy (LDA), including quasi-relativistic correction, *vs.* total spin for $[M_2Cl_9]^{3-}$ [M = Mo (△) or W (○)] systems calculated with and without (▲, ●) NL gradient corrections

the spin-triplet species (S_{max} = 1) results in greater destabilization for $[W_2Cl_9]^{3-}$ compared to $[Mo_2Cl_9]^{3-}$ by 6.1 kcal mol^{-1} when the LDA with relativistic corrections are used. This relative destabilization of $[W_2Cl_9]^{3-}$ then increases as a function of total spin to 12.5 (S_{max} = 2) and finally 19.9 kcal mol^{-1} (S_{max} = 3). This result can be interpreted in terms of the relative accessibility of the higher-spin states in these two systems since a given spin state will always be more energetically accessible for $[Mo_2Cl_9]^{3-}$ than $[W_2Cl_9]^{3-}$.

Fragment analysis

A series of fragment calculations,[26] incorporating both non-local gradient and quasi-relativistic corrections, were undertaken in order to pinpoint the factors behind the different relative energies of the excited spin levels of $[Mo_2Cl_9]^{3-}$ and $[W_2Cl_9]^{3-}$. As noted above, the inclusion of non-local gradient corrections makes negligible difference when comparing the relative energies of the excited-spin states for Mo and W. In both systems unpairing the electron-spin density causes drastic lengthening of the M–M bond. In the analysis, therefore, it is necessary to account not only for the consequences of electron unpairing, but also for the effect of increasing M–M distance on the bonding in the system. This latter point has been discussed before by Summerville and Hoffmann.[7] In their extended-Hückel study they indicated that full occupation of the M–M manifold (for example, in a d^6–d^6 dimer) would lead to elongation of the dimer and an increase in the M–M distance. Geometries resulting from partial occupation of the M–M manifold were dependent on several factors: the strength of the direct M–M interaction, the interaction with the bridging halides and the steric repulsion between ligands. They concluded that the shortening of the M–M distance seen in $[M_2Cl_9]^{3-}$ species (M = Cr, Mo or W) as the triad is descended was due to the increasing M–M overlap which favoured M–M bond formation and compression of the structure.

In our study two series of fragment calculations were conducted to investigate the effects of unpairing electron-spin density and increasing the M–M separation in $[Mo_2Cl_9]^{3-}$ and $[W_2Cl_9]^{3-}$. These calculations follow the approach of Summerville and Hoffmann by fragmenting the molecule into two terminal $\{MCl_3\}$ units and a bridging $\{Cl_3\}^{3-}$ unit. This allows the dimer to be reconstructed in a stepwise fashion and enables an examination, first, of the direct metal–metal interaction arising from the formation of the $\{M_2Cl_6\}$ fragment from two terminal $\{MCl_3\}$ units and then the metal–bridge interaction by constructing the final $[M_2Cl_9]^{3-}$ molecule from $\{M_2Cl_6\}$ and $\{Cl_3\}^{3-}$ fragments.

Effect of electron promotion at a constant geometry. In the first series of calculations the terminal $\{MCl_3\}$ units were maintained at the geometry optimized for the spin-singlet species for each metal while the geometry of the $\{Cl_3\}^{3-}$ bridge unit was averaged from those calculated for the spin-singlet species of $[Mo_2Cl_9]^{3-}$ and $[W_2Cl_9]^{3-}$. The $\{MCl_3\}$ units were placed at the average M–M separation of 2.321 Å found for the spin-singlet species. The dimer energies were then calculated at this geometry, varying the electron occupation of the M–M manifold to produce spin-singlet, -triplet, -quintet and -septet species in both the $\{M_2Cl_6\}$ fragments and the final $[M_2Cl_9]^{3-}$ molecules. Spin-restricted calculations were performed on the $\{MCl_3\}$ and $\{M_2Cl_6\}$ fragments, corresponding to a spin-averaged occupation of the M–M based frontier orbitals, whereas spin-unrestricted calculations were undertaken on the $[M_2Cl_9]^{3-}$ dimer.

Table 3 gives the metal–metal, metal–bridge and total interaction energies as a function of total spin at a constant geometry. For the spin-singlet species the metal–metal interaction is stronger for $[W_2Cl_9]^{3-}$ by 28.8 kcal mol^{-1}. The metal–bridge interaction on the other hand is very similar for the spin-singlet species in both systems. As the metal–metal bonding electrons are unpaired, a steady reduction in the strength of the metal–metal interaction is computed for both systems. However, as the total spin increases, the extent to which the metal–metal interaction is stronger in $[W_2Cl_9]^{3-}$ compared to $[Mo_2Cl_9]^{3-}$ is reduced to 19.4 (S_{max} = 1) and 9.2 kcal mol^{-1} (2), until for S_{max} = 3 the metal–metal interaction is only 1.1 kcal mol^{-1} stronger. The metal–bridge interaction remains very similar for both systems in the higher-spin states and is increasingly stabilized as the total spin increases. Thus, the occupation of the metal–metal antibonding orbitals apparently enhances the metal–bridge interaction.

The above analysis shows that, at a constant M–M separation, the contributions from the metal–metal and –bridge interactions counteract each other, with the destabilization due to loss of metal–metal bonding being greater than the stabilization of the metal–bridge interaction in the higher total-spin species. In addition, changes in the metal–metal interaction as the total spin increases are less destabilizing for $[Mo_2Cl_9]^{3-}$.

The trends in metal–metal interaction can be simply understood in terms of the overlap of the metal-based orbitals, with the greater overlap between the two tungsten centres leading to stronger metal–metal bonding in the case of $[W_2Cl_9]^{3-}$. However, as electrons are promoted, first from the e′ to e″ orbitals and then from a_1' to a_2'', the orbitals which are more strongly M–M bonding are depopulated while orbitals which are more strongly M–M antibonding are populated. The $[W_2Cl_9]^{3-}$ system therefore loses more M–M bonding stabilization as a consequence of this electron redistribution than does $[Mo_2Cl_9]^{3-}$.

Understanding the increased stabilizing metal–bridge interaction in the excited-spin states is not so straightforward. The metal–bridge bonding occurs through electron donation from the bridge orbitals to vacant metal-based orbitals of the $\{M_2Cl_6\}$ unit. In the spin-singlet species the e″ and a_2'' metal-based orbitals are available to act as acceptors from occupied bridge orbitals of appropriate symmetry. To higher energy lie more metal-based acceptor orbitals,[7] but as neither the geometry of the molecule nor the occupations of these acceptor orbitals is changing in these calculations, donation into these orbitals is expected to be constant. Also, in the spin-singlet species the occupied a_1' and e′ orbitals undergo 4e destabilizations with occupied bridge orbitals of appropriate symmetry. As an electron is promoted from e′ to e″ the

Table 3 Variation in metal–metal, metal–bridge and total interaction energies (kcal mol^{-1}) with total spin for $[M_2Cl_9]^{3-}$ (M = Mo or W) at an average singlet geometry (M–M 2.321 Å)

	Metal–metal		Metal–bridge		Total*	
S_{max}	Mo	W	Mo	W	Mo	W
0	−112.3	−141.1	−263.1	−252.4	−387.2	−405.3
1	−76.2	−95.6	−273.6	−263.2	−361.6	−370.6
2	−35.9	−45.1	−302.4	−291.9	−350.1	−348.8
3	+47.3	+46.2	−317.5	−303.1	−282.0	−268.7

* Includes a constant term for the formation of the $\{Cl_3\}^{3-}$ bridging unit.

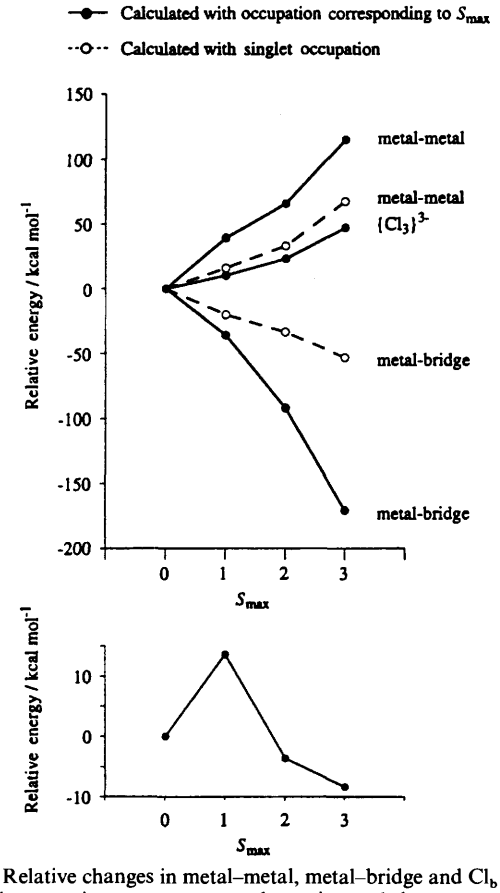

Fig. 4 Relative changes in metal–metal, metal–bridge and $Cl_b \cdots Cl_b$ interaction energies upon geometry elongation and electron promotion for $[Mo_2Cl_9]^{3-}$. Plot at bottom corresponds to sum of above interaction energies (solid curves) *vs.* total spin

donation into the e″ orbital is necessarily interrupted. However, the 4e destabilization involving one of the e′ orbital pair, which is now only half occupied, is to some extent relieved and donation into this orbital may occur. The calculations indicate that these latter considerations are more significant, outweighing the reduction in acceptor ability of the e″ orbital, and result in a net stabilization of the metal–bridge interaction. This may simply be a result of the energy mismatch between the bridge donor orbitals with the metal fragment orbitals as the metal-based e′ orbital is lower in energy than the e″ and so interacts more strongly with the bridge orbitals.

Effect of electron promotion with geometry elongation. The second series of fragment calculations involved an analysis of the changes that occur when the molecule is elongated and the electrons reorganized in the M–M manifold. These calculations were performed on spin-triplet, -quintet and -septet structures averaged in a similar way to those used in the analysis of the spin-singlet structure above. Thus, the M–M and $Cl_b \cdots Cl_b$ distances from the molybdenum and tungsten structures optimized for each total spin state were averaged. For these average geometries two calculations were performed, the first with an electron occupation equivalent to a spin-singlet state and the second with an occupation appropriate for the geometry under study. In order to pinpoint the factors that determine the energy trends in these systems, the terminal $\{MCl_3\}$ units were maintained at the geometry found in the spin-singlet structures of $[Mo_2Cl_9]^{3-}$ and $[W_2Cl_9]^{3-}$. The geometries employed are given in Table 4, as well as the relative changes in the metal–metal and –bridge interaction energies, the relative energies for the formation of the $\{Cl_3\}^{3-}$ bridge fragment and the relative total interaction energies. This two-step analysis allows one to assess first the effects of changes in geometry from that of the optimized spin-singlet structure and then the effects of electron reorganization at that geometry.

This approach is illustrated for the case of $[Mo_2Cl_9]^{3-}$ (Fig. 4). Three effects are considered. First, the $\{Cl_3\}^{3-}$ bridge unit is destabilized in the higher total-spin states. This is a consequence of the longer M–M separation in these species, resulting in a decrease in the $Cl_b \cdots Cl_b$ non-bonded distance and, therefore, increased steric repulsion between the Cl_b ions. Secondly, the dashed curves plot the loss of metal–metal interaction (destabilizing) and the enhanced metal–bridge interaction (stabilizing) calculated for a spin-singlet occupation of the elongated structures. As before, increasing the metal–metal distance reduces the metal–metal bonding interaction. Elongation also increases the metal–bridge interaction, due mainly to better overlap between the metal-based a_2'' and e″ acceptor orbitals and their symmetry equivalents on the $\{Cl_3\}^{3-}$ unit.[7] For a spin-singlet occupation the destabilizing effects of $Cl_b \cdots Cl_b$ steric interference and loss of metal–metal bonding outweigh the stabilizing metal–bridge interaction and elongation results in overall destabilization. The solid curves in Fig. 4 correspond to the metal–metal and metal–bridge interactions upon electron reoccupation to give the appropriate excited-spin state. Significant further reduction in the metal–metal bonding interaction is calculated upon electron promotion, as was the case in the constant-geometry calculations discussed above. Electron promotion also results in significant stabilization of the metal–bridge interaction, particularly for the $S_{max} = 2$ and 3 levels. Finally, at the bottom of Fig. 4, the energy contributions from the $\{Cl_3\}^{3-}$ bridge unit, the metal–metal and metal–bridge interactions (corresponding to the solid curves in Fig. 4) have been summed to give the total energy of the system and plotted against S_{max}. This yields the same overall shape for the S_{max} *vs.* energy profile for the fully optimized structures of $[Mo_2Cl_9]^{3-}$ (*cf.* Fig. 3) indicating that the approximations in our analysis have not affected the underlying trends. The results of an equivalent analysis for $[W_2Cl_9]^{3-}$ are similar to those described above for $[Mo_2Cl_9]^{3-}$.

The data in Table 4 serve to identify the factors behind the different relative energies calculated for the excited-spin states of $[W_2Cl_9]^{3-}$ and $[Mo_2Cl_9]^{3-}$. The total energies of the spin-singlet species indicate that $[W_2Cl_9]^{3-}$ undergoes more rapid destabilization upon elongation than does $[Mo_2Cl_9]^{3-}$. This is due to the greater loss of metal–metal interaction for $[W_2Cl_9]^{3-}$ in the elongated structures coupled with the metal–bridge interaction, which is intrinsically stronger for $[Mo_2Cl_9]^{3-}$. Even without electron promotion, therefore, geometry elongation is more destabilizing for $[W_2Cl_9]^{3-}$.

Unpairing the metal–metal bonding electrons reinforces the trends described above for geometry elongation. In the excited-spin states the calculations predict a further stabilization of the metal–bridge interaction and an increased loss of metal–metal interaction. However, while the stabilization of the metal–bridge interaction upon electron promotion is rather similar for both metals, the loss of metal–metal interaction is larger for $[W_2Cl_9]^{3-}$. This effect is the major contributing factor to the higher relative energies of the excited-spin states of $[W_2Cl_9]^{3-}$. Thus, both the geometry elongation and electron promotion

Table 4 Relative changes in metal–metal, metal–bridge, $\{Cl_3\}_3$ and total interaction energies (kcal mol^{-1}) as a function of total spin and geometry (Å) for $[M_2Cl_9]^{3-}$ (M = Mo or W)

	Geometry		Metal–metal interaction		Metal–bridge interaction			Total interaction energy	
S_{max}	M–M	$Cl_b \cdots Cl_b$	Mo	W	Mo	W	$\{Cl_3\}_3$	Mo	W
0	2.321	3.933	0.0	0.0	0.0	0.0	0.0	0.0	0.0
0	2.605	3.756	+15.9	+9.9	−20.2	−14.2	+10.2	+5.9	+5.9
0	2.862	3.563	+33.1	+29.0	−33.7	−24.8	+22.9	+22.3	+27.1
0	3.478	3.255	+67.6	+74.2	−53.3	−46.6	+47.3	+61.6	+74.9
1	2.605	3.756	+39.3	+39.3	−35.9	−30.0	+10.2	+13.6	+19.5
2	2.862	3.563	+65.6	+70.5	−92.1	−84.1	+22.9	−3.6	+9.3
3	3.478	3.255	+115.0	+136.0	−170.6	−170.7	+47.3	−8.3	+12.6

result in a greater loss of metal–metal bonding in the excited-spin states of $[W_2Cl_9]^{3-}$ compared to $[Mo_2Cl_9]^{3-}$ and both factors can be traced to the stronger metal–metal interaction in the spin-singlet species of $[W_2Cl_9]^{3-}$.

The data in Table 4 also allow the pattern of relative energies of the excited-spin states of $[Mo_2Cl_9]^{3-}$ and $[W_2Cl_9]^{3-}$, calculated using the non-local gradient corrections, to be understood. Fig. 3 indicates that, for both metals, the spin triplet is the most unstable excited-state species. Subsequent electron promotion may have been expected to produce further destabilization, but the resultant spin-quintet and -septet species are in fact stabilized relative to the spin-triplet species. The fragment analysis shows that although the metal–metal and $Cl_b \cdots Cl_b$ interaction terms are both strongly destabilizing in the excited-spin states, this destabilization is counteracted by the metal–bridge interaction. The factors that favour an increased metal–bridge interaction are an elongated geometry and a high total spin. For the spin-triplet species neither condition is satisfied and consequently the metal–bridge interaction is not sufficiently stabilized to counteract the loss of metal–metal bonding and increased $Cl_b \cdots Cl_b$ steric interaction. This results in the large destabilization of the spin-triplet species relative to the singlet. For $S_{max} = 2$ and 3 the higher total spin and more elongated geometries result in a greater stabilization of the metal–bridge interaction and lower relative energies for the spin-quintet and -septet structures compared to those of the spin-triplet species.

Comments on the structures of $A_3M_2Cl_9$ species

The experimentally determined Mo–Mo distances in $A_3Mo_2Cl_9$ systems show a remarkable dependence on the size of the univalent cation, A (see Table 2), with the Mo–Mo separation increasing with size of the A cation. The fact that this effect is so dramatic has been taken as a reflection of an intermediate metal–metal interaction, consistent with the detailed spectroscopic analysis of $Cs_3Mo_2Cl_9$,[5] which means that small changes in solid-state packing can have a significant effect on the Mo–Mo distance. A comparison of the known structures of $A_3W_2Cl_9$ (A = K, W–W 2.41 Å; A = Cs, W–W 2.50 Å) shows that variation in the W–W distance with the A cation size can occur even for apparently strongly interacting metal centres. The effect is larger for $[Mo_2Cl_9]^{3-}$, where a lengthening of 0.16 Å is observed between the potassium and caesium salts compared to 0.09 Å for $[W_2Cl_9]^{3-}$. The calculations indicate that for both metal systems the excited-spin species lie relatively close in energy to the spin-singlet species. However, as pointed out previously, the spin-triplet configuration does not correspond to a pure spin state. Thus, the destabilization of the spin-quintet and -septet species relative to the spin-singlet species is a more reliable measure of the energy difference between the ground state and the low-lying excited-spin states. From the relativistic LDA total energies given in Table 1, the spin-quintet and -septet species lie approximately 12.4 and 21.6 kcal mol^{-1}, respectively, above the spin-singlet species for $[Mo_2Cl_9]^{3-}$. The corresponding values for $[W_2Cl_9]^{3-}$ are 24.9 and 41.6 kcal mol^{-1}, respectively. Thus, the facile variation in M–M distances in both these species may be explained by the presence of low-lying excited-spin states which can be accessed *via* small changes in solid-state packing. The observation that $[Mo_2Cl_9]^{3-}$ is more sensitive to the A cation size than is $[W_2Cl_9]^{3-}$ is consistent with the results of our calculations which indicate that the excited-spin states are lower in energy for $[Mo_2Cl_9]^{3-}$ and therefore more accessible than for $[W_2Cl_9]^{3-}$.

Conclusion

The geometries and relative energies of the ground ($S_{max} = 0$) and excited ($S_{max} = 1$–3) spin states for $[Mo_2Cl_9]^{3-}$ and $[W_2Cl_9]^{3-}$ have been calculated using density-functional methods incorporating relativistic effects. Significant M–M elongation with increasing dimer spin state occurs for both systems with the spin-singlet species predicted to be the most stable when the local-density approximation is used. When non-local corrections to the total energy are included both the spin-quintet and -septet species of $[Mo_2Cl_9]^{3-}$ are calculated to be more stable than the spin singlet. The calculated W–W separation of 2.404 Å for the spin-singlet species of $[W_2Cl_9]^{3-}$ is in good agreement with experimental data. In the case of $[Mo_2Cl_9]^{3-}$, the calculated Mo–Mo distance of 2.612 Å for the spin-triplet species is within the range of experimental distances, the calculated spin-singlet separation being too short. Fragment calculations on both $[Mo_2Cl_9]^{3-}$ and $[W_2Cl_9]^{3-}$ reveal that the changes in the metal–metal and metal–bridge interactions counteract each other in the higher spin-state species. Electron promotion within the M–M manifold leads to a loss of metal–metal bonding and a stronger metal–bridge interaction. The calculations indicate that the higher-spin states are more accessible for $[Mo_2Cl_9]^{3-}$ than for $[W_2Cl_9]^{3-}$ consistent with the more dramatic variation in metal–metal distances observed in $A_3Mo_2Cl_9$ complexes.

Acknowledgements

The Australian Research Council (ARC) is gratefully acknowledged for financial support (to R. S.). We also thank the EPSRC (UK) for the provision of an overseas studentship (to T. L.).

References

1 F. A. Cotton and R. A. Walton, *Multiple Bonds between Metal Atoms*, 2nd edn., Clarendon Press, Oxford, 1993.
2 F. A. Cotton and D. A. Ucko, *Inorg. Chim. Acta*, 1972, **6**, 161.
3 R. Saillant and R. A. D. Wentworth, *Inorg. Chem.*, 1968, **7**, 1606; G. J. Wessel and D. J. W. Ijdo, *Acta Crystallogr.*, 1957, **10**, 466; I. E. Grey and P. W. Smith, *Aust. J. Chem.*, 1971, **24**, 73.
4 K. R. Dunbar and L. E. Pence, *Acta Crystallogr., Sect. C*, 1991, **47**, 23; W. H. Watson, jun. and J. Waser, *Acta Crystallogr.*, 1958, **11**, 689.

5 (*a*) L. Dubicki, E. R. Krausz, R. Stranger, P. W. Smith and Y. Tanabe, *Inorg. Chem.*, 1987, **26**, 2247; (*b*) R. Stranger, I. E. Grey, I. C. Madsen and P. W. Smith, *J. Solid State Chem.*, 1987, **69**, 162; (*c*) R. Stranger, *Chem. Phys. Lett.*, 1989, **157**, 472; (*d*) R. Stranger, P. W. Smith and I. E. Grey, *Inorg. Chem.*, 1989, **28**, 1271; (*e*) R. Stranger, G. Moran, E. R. Krausz, L. Dubicki, H. Güdel and N. Furer, *Inorg. Chem.*, 1992, **31**, 2860; (*f*) R. Stranger, G. Moran, E. R. Krausz, G. A. Medley and H. Güdel, *Inorg. Chem.*, 1993, **32**, 4555; (*g*) R. Stranger, *Inorg. Chem.*, 1990, **29**, 5231; (*h*) R. Stranger, L. Dubicki and E. R. Krausz, *Inorg. Chem.*, 1996, **35**, 418.
6 G. A. Medley and R. Stranger, *Inorg. Chem.*, 1994, **33**, 3976.
7 R. H. Summerville and R. Hoffmann, *J. Am. Chem. Soc.*, 1979, **101**, 3821.
8 G. A. Heath and J. E. McGrady, *J. Chem. Soc., Dalton Trans.*, 1994, 3767.
9 A. P. Ginsberg, *J. Am. Chem. Soc.*, 1980, **102**, 111.
10 H. Jacobsen, H.-B. Kraatz, T. Ziegler and P. M. Boorman, *J. Am. Chem. Soc.*, 1992, **114**, 7851.
11 F. A. Cotton and X. Feng, *Int. J. Quantum Chem.*, 1996, **58**, 671.
12 T. Lovell, J. E. McGrady, R. Stranger and S. A. Macgregor, *Inorg. Chem.*, 1996, **35**, 3079.
13 (*a*) R. G. Parr and W. Yang, *Density-functional Theory of Atoms and Molecules*, Clarendon Press, New York, 1989; (*b*) T. Ziegler, *Chem. Rev.*, 1991, **91**, 651.
14 E. J. Baerends, D. E. Ellis and P. Ros, *Chem. Phys.*, 1973, **2**, 41; E. J. Baerends, J. G. Snijders, C. A. de Lange and G. Jonkers, *Local Density Approximations in Quantum Chemistry and Solid State Physics*, eds. J. P. Dahl and J. Avery, Plenum, New York, 1984.
15 P. M. Boerrigter, G. te Velde and E. J. Baerends, *Int. J. Quantum Chem.*, 1988, **33**, 87.
16 G. J. Snijders, E. J. Baerends and P. Vernooijs, *At. Data Nucl. Data Tables*, 1982, **26**, 483; P. Vernooijs, G. J. Snijders and E. J. Baerends, *Slater Type Basis Functions for the whole Periodic System*, Internal Report, Free University of Amsterdam, 1981.
17 J. Krijn and E. J. Baerends, *Fit Functions in the HFS-method*, Internal Report, Free University of Amsterdam, 1984.
18 E. J. Baerends, D. E. Ellis and P. Ros, *Theor. Chim. Acta*, 1972, **27**, 339.
19 O. Gunnarsson, B. I. Lundquist and J. W. Wilkins, *Phys. Rev. B*, 1974, **10**, 1319; O. Gunnarsson and B. I. Lundquist, 1976, **13**, 4274; O. Gunnarsson, M. Johnson and B. I. Lundquist, *Phys. Rev. B*, 1979, **20**, 3136.
20 S. J. Vosko, M. Wilk and M. Nusair, *Can. J. Phys.*, 1980, **58**, 1200.
21 L. Versluis and T. Ziegler, *J. Chem. Phys.*, 1988, **88**, 322.
22 T. Ziegler, V. Tschinke, E. J. Baerends, J. G. Snijders and W. Ravenek, *J. Phys. Chem.*, 1989, **93**, 3050.
23 J. P. Perdew, J. A. Chevary, S. H. Vosko, K. A. Jackson, M. R. Pederson, D. J. Singh and C. Fiolhais, *Phys. Rev. B*, 1992, **46**, 6671.
24 T. Ziegler and L. Fan, *J. Chem. Phys.*, 1991, **95**, 7401.
25 P. D. Lyne and D. M. P. Mingos, *J. Chem. Soc., Dalton Trans.*, 1995, 1635; K. H. Moock, S. A. Macgregor, G. A. Heath, S. Derrick and R. T. Boere, *J. Chem. Soc., Dalton Trans.*, 1996, 2067.
26 T. Ziegler, *NATO ASI., Ser. C*, 1992, **378**, 367.

Received 25*th March* 1996; *Paper* 6/02042I